Chemical Physics 349 (2008) 296–307

Contents lists available at ScienceDirect

Chemical Physics

journal homepage: www.elsevier.com/locate/chemphys

Pulse-train control of multiphoton transitions in anharmonic progressions: Resonance loci and resonance ridges

Markus Seidl, Christoph Uiberacker [1], Werner Jakubetz *

University of Vienna, Department of Theoretical Chemistry, Währinger Straße 17, 1090 Wien, Austria

ARTICLE INFO

Article history:
Received 14 January 2008
Accepted 20 February 2008
Available online 5 March 2008

Keywords:
Pulse train
Multiphoton excitation
Pi-pulse
Control

ABSTRACT

The properties of pulse-train induced multiphoton excitation in anharmonic progressions and the accumulation of population in a specific rung state are investigated by means of numerical simulations. It is shown how and under which conditions resonant π-pulses and multiple-π pulses can be split into trains of fractional π-pulses driving the same transition. Standardized train forms are considered with sub-pulses of equal (gaussian) shapes and equal, but tunable pulse-to-pulse delays and pulse-to-pulse phase shifts. The increased number of tuning parameters together with the handle on the number of sub-pulses gives rise to a remarkable variability in the control of state-specific population transfer, where simple zero-order estimates assist the determination of the parameters. Each π- or multiple-π pulse is replaced by a resonance locus in parameter space representing an infinite set of π-trains. The loci span extended frequency ranges that increase with increasing sub-pulse number. Their projection onto the frequency-field strength plane gives rise to elliptically shaped closed curves, termed resonance ridges, which replace the singular points mapped out by simple π- and multiple-π pulses. In the subspace of pulse-to-pulse delays and pulse-to-pulse phase shifts the resonance loci are characterized by phase recurrence relations, whose number and complexity increases with increasing numbers of sub-pulses. Our results indicate that pulse trains may be a powerful tool for the control of parallel or branching multiphoton transitions and for the elimination of background and intruder state population.

1. Introduction

In *N*-level systems (NLSs), pulse trains can be used to accumulate population in pre-selected levels [1–10]. This aspect of population control has been studied in particular for population transfer in 2-level systems (2LSs) [1–3,9] and in harmonic and anharmonic *N*-level progressions [4–8]. In dipolar systems, this mechanism also covers multiphoton (mp) transitions without intermediate levels, *e.g.* in 2LSs [9]. Recently, trains of pulse pairs effecting adiabatic passage in pump–dump transitions have been considered [10].

The findings in these investigations imply that in effect a (generalized) π-pulse [11–14] driving specific transitions may be replaced by a train of properly adjusted fractional π-pulses. The additional parameters characterizing pulse trains, most prominently the pulse-to-pulse (ptp) time delays and the ptp-phase shifts, together with the number of sub-pulses, provide new handles for the control of state-specific population transfer. In this context, a highly useful feature is the possibility to achieve full population transfer for detuned frequencies over a range whose size varies with the number of sub-pulses [1].

The purpose of the present paper is to explore in detail the properties of pulse-train driven mp ladder climbing along anharmonic progressions as well as the limitations of the method. We split resonant π-pulses into trains of fractional π-pulses and determine the conditions, under which constructive superposition gives rise to accumulation of population in the target state. In particular, we investigate the conditions on the ptp time delays and ptp phase shifts that allow the design of "π-trains" as equivalents of simple π-pulses, *i.e.* trains that *overall* act like π- or multiple-order π-pulses. While pulse-train control of population transfer in simple anharmonic progressions has been considered before [4–8], we take an extended look at this problem by way of numerical simulations, in which we address aspects that are important as reference for pulse-train control in more complex situations. We thereby extend the analytical results for 2LSs obtained Vitanov and Knight [1] within the rotating wave approximation (RWA) [11,14] to mp processes in NLSs, dropping the RWA in view of expected shortcomings under these more demanding conditions [15,16]. Note by working with trains of fractional π-pulses we use only the Fourier

* Corresponding author. Tel.: +43 1 4277 52758; fax: +43 1 42779527.
E-mail address: werner.jakubetz@univie.ac.at (W. Jakubetz).
[1] Present address: Institute for Physics, University of Leoben, 8700 Leoben, Austria.

0301-0104/$ - see front matter © 2008 Elsevier B.V. All rights reserved.
doi:10.1016/j.chemphys.2008.02.058

frequency components coming from the individual sub-pulses, and do not exploit the properties of the associated frequency comb [17]. Use of the latter has been suggested as a means for achieving ultrahigh vibrational excitation in anharmonic progressions [18–20]. Ultimately, our goal is to employ pulse trains as a tool for controlling parallel or branching processes. If the competing processes differ in photonicity or involve near-degenerate transitions, their different response to the ptp-characteristics of pulse trains will allow separating the processes.

The present paper is organized as follows. In Section 2 we introduce our model systems. In Section 3 we describe the properties of resonant π-pulses and pulse trains. We restrict our attention to what we denote "*m*-trains" as trains of *m* non-overlapping gaussian sub-pulses [21,22] with identical shapes, amplitudes, central frequencies, ptp time delays and ptp phase shifts. We deal with the role of the number of sub-pulses, identifying two regimes corresponding to "few" and "many" sub-pulses. In Section 4 we summarize results obtained from numerical solutions of the Schrödinger equation. We first deal with simple π-pulses, which form the reference frame for the design of π-trains. We then present our results for pulse-train control. In particular, we explore the properties of π-trains, and the conditions under which control can be robust with respect to any of the control parameters. We characterize 4-dimensional resonance loci in parameter space comprising infinite sets of π-trains, and resonance ridges as their projections onto the amplitude–frequency plane. We then address multiple-order π-trains, and show that the resonance loci of π-trains of different order are coupled and connected. Finally, in Section 5 we present our conclusions and discuss the implications for pulse-train control of branching or parallel processes.

2. The model *N*-level ladder systems

In this section, we describe the specific NLSs that are used in our simulations. As illustrated in Fig. 1, our systems are sequentially coupled anharmonic progressions of *N* levels $|1\rangle$ to $|N\rangle$. For $N = 3$–6, respectively, we abbreviate our systems 3LS, 4LS, 5LS, and 6LS. The corresponding level energies are denoted ε_1 to ε_N, and are given by a Morse progression, where in each system the uppermost rung spacing $(\varepsilon_N - \varepsilon_{N-1})$ is set to 0.00425 a.u.,[2] and consecutively lower level spacings are incremented by 0.00025 a.u. These values are adapted from the HCN bend state progression [23], so that our results can be related to a typical molecular situation. However, the results are in fact more general and by invoking reduced units they will also scale to different frequency regimes.

Furthermore, for the 3LS we explore the consequences of "embedding" the ladder states into a longer anharmonic progression by adding one level below $|1\rangle$ (denoted $|-\rangle$), and one level above $|N\rangle$ (denoted $|+\rangle$). Fig. 1 includes a sketch of this embedding extension. Nominally it defines a 5-level system, for which we use the notation "embedded 3LS". The findings for the embedded system carry over to the larger systems, for which embedding extensions are not considered explicitly.

In order to use a notation that is independent of the specific system, we will also denote, interchangeably, level $|1\rangle$ as *initial* state $|\mathrm{I}\rangle$ and level $|N\rangle$, the target state of the $(N-1)$-photon transitions to be driven, as *final* state $|\mathrm{F}\rangle$.

The zero-order resonance frequencies of the $(N-1)$-photon transitions $|\mathrm{I}\rangle \rightarrow |\mathrm{F}\rangle$ are

$$\omega_0^{\mathrm{IF}} = (\varepsilon_{\mathrm{F}} - \varepsilon_{\mathrm{I}})/(N-1)\hbar. \tag{1}$$

For a pulse or pulse train at central frequency ω, the individual levels $|j\rangle$ of the anharmonic ladder (with zero-order transition frequencies $\omega_0^{\mathrm{I}j}$) are detuned by $\mathrm{d}\varepsilon_j$ (denoted "rung detuning"), and

$$\mathrm{d}\varepsilon_j = |(\varepsilon_j - \varepsilon_1) - (j-1)\omega|. \tag{2}$$

For the special case $\omega = \omega_0^{\mathrm{IF}}$, we have

$$\mathrm{d}\varepsilon_j^0 = |(\varepsilon_j - \varepsilon_1) - (j-1)\omega_0^{\mathrm{IF}}|. \tag{3}$$

It is our objective to study the phenomena associated with pulse-train control in a systematic way. Therefore all NLSs are assumed to be non-polar and to be purely sequentially coupled, so that for the elements of the $N \times N$ dipole matrix **M** we have

$$\mu_{ij} = \mu_{ji} = \begin{cases} \mu_{\mathrm{L}}, & i = 1,\ldots,N-1,\ j = i+1, \\ 0, & \text{else.} \end{cases} \tag{4}$$

The value $\mu_{\mathrm{L}} = 0.2$ a.u., adapted from the bend progression of the HCN molecule [25–27], is used throughout. Dropping the simplifications in **M** by including permanent dipole moments and overtone couplings, as *e.g.* in realistic *molecular* systems, does not lead to significant changes in the control properties, and all phenomena described in the following sections are still observed. However, in this case their appearance can be obscured by effects arising from interference with alternative excitation pathways that involve direct or dipole-induced [28–30] overtone transitions. Characteristic properties of the systems are shown in Table 1.

3. Pulse-train driven multiphoton ladder climbing

3.1. Resonant excitation by simple pulses

We first consider a state-specific *k*-photon transition in an anharmonic $(k+1)$-level progression driven by a pulse of given shape and length. In particular, we use pulses with gaussian envelopes, which we characterize by the pulse length T_{p}, the full-width at half-height (fwhh) in field strength; the width of the intensity envelope is narrower by a factor $\sqrt{0.5}$. Under these conditions, resonance occurs at frequency $\omega_{\mathrm{r}}^{\mathrm{IF}}$, displaced from the zero-order transition frequency ω_0^{IF} by the Bloch–Siegert shift [31,32] γ^{IF}.[3] The corresponding peak amplitude of the gaussian envelope is A_{r}. With the typical molecular parameters used for our model systems, the shortest time domain for which the situation described above obtains is the T_{p} range of one to few picoseconds. For pulses in the sub-picosecond domain the spectral width of the pulses covers the anharmonic detunings of intermediate rung states, allowing final population of such states and destroying state-specificity. In view of this situation, throughout this paper we use a standard value $T_{\mathrm{p}} = 8$ ps. A resonant process will be understood to mean that the initial state population P_{I} is numerically zero at the end of the pulse.

In the time regime of few picoseconds and for low photonicities, γ^{IF} remains reasonably small, and the population dynamics show a nearly unperturbed Rabi-type [11,14,33] sinusoidal variation of and P_{I} and the final state population P_{F}, with at most small transient contributions from intermediate rung states. It is important to note that under the conditions laid out, and provided it is possible at all, for fixed T_{p} two pulse parameters (*i.e.* $\omega_{\mathrm{r}}^{\mathrm{IF}}$ and A_{r}) are required to achieve the avoided crossing conditions among instantaneous Floquet quasienergy states [34] that define a generalized π-pulse [13] or higher-order $n\pi$-pulse, and that the *n*-dependent pairs $(\omega_{\mathrm{r}}^{\mathrm{IF}}, A_{\mathrm{r}})$ represent a set of discrete points in the (ω, A_0)-plane.

[2] For the characterization of our NLSs and laser fields we use atomic units (a.u.), with the following conversion factors [24]: 1 a.u. of energy = 1 hartree = 4.35981×10^{-18} J, 1 a.u. of circular frequency = 6.57968×10^{15} Hz (corresponding to a wavenumber of 219,474 cm^{-1}), 1 a.u. of field strength = 514.225 GV m^{-1}, and 1 a.u. of dipole moment = 2.54176 D = 8.47841×10^{-30} C m.

[3] We use the term "Bloch–Siegert shift" generally for any field-induced resonance shift in pulse-driven transitions in *N*-level systems. The term is often used more restrictively, see *e.g.* Refs. [14,31,32].

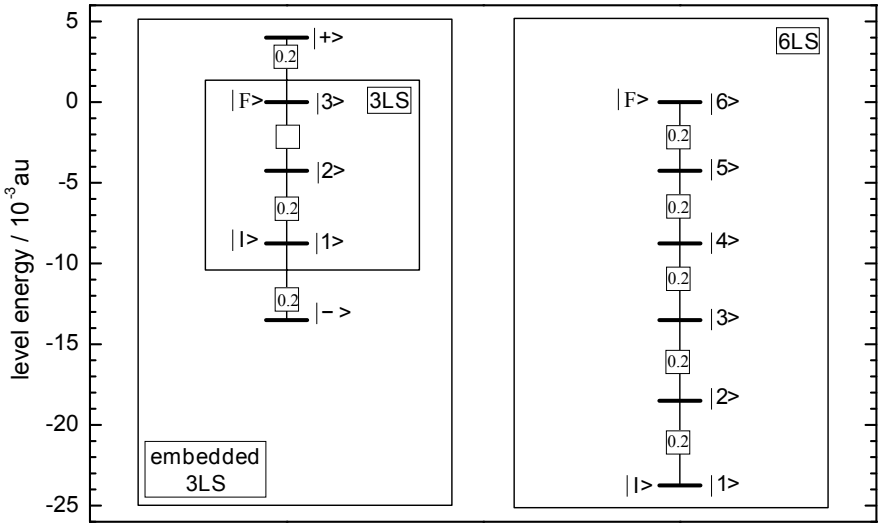

Fig. 1. Level diagrams and notation for the model systems. Left: the 3-level and embedded 3-level systems. Right: the 6-level system. The energies of the anharmonic progression are to scale. The levels are sequentially coupled by transition dipole moments of 0.2 a.u.

Table 1
Properties of the model anharmonic ladder systems

System	3LS	emb. 3LS	4LS	5LS	6LS
ω_0^{IF} [a]	.004375	.004375000$_1$	.004500	.004625	.004750
ε_{min} [b]	.000125	.000125	.000250	.000375	.000500
m_{sw} [c]	5	5	10	15	20

[a] Zero-order resonance frequency (circular frequency in a.u.) for $(N-1)$-photon transition in the NLS system.
[b] Smallest rung-state detuning (energy in a.u.) at zero-order frequency ω_0^{IF}.
[c] Switch-over sub-pulse number from m-regime I to II: estimated onset of rung-state participation for m-trains with $T_p = 8$ ps and central frequency ω_0^{IF}; from Eqs. (6) and (7).

3.2. Resonant excitation by pulse trains

We now split the driving π-pulse into m equal and equally spaced sub-pulses [1], again with gaussian shape [21,22], width (fwhh) $T_m = T_P/m$, ptp time delay Δ_{ptp}, ptp-phase shift δ_{ptp}, frequency ω and sub-pulse amplitude A_0. Except for T_m, the parameters are left unspecified for the moment, but we may assume that ω and A_0 are, respectively, close to ω_r^{IF} and A_r. Furthermore, Δ_{ptp} is limited (from below) by the requirement that the sub-pulses should be effectively non-overlapping. If Δ_{ptp} is chosen as small as possible complying with this condition, then the entire m-train of densely spaced, but non-overlapping sub-pulses covers about the same time span as the original π-pulse, so that no *additional* phenomena such as rotational motion or spontaneous emission are introduced. Although the experimental design of such closely spaced sub-pulses is out of reach of present technology, we will stick to this vision of a control tool. Pulse trains approaching the nanosecond time scale clearly offer less exciting control prospects.

The condition of effectively non-overlapping gaussian sub-pulses is approximately fulfilled for $\Delta_{ptp} > 2.5\ T_m$, which for the standard parameters used means $\Delta_{ptp} > 20/m$ ps. Down to this value the results from the simulations retain their regular patterns.

We call a uniform sequence of m non-overlapping pulses as described above an "m-train" (a 4-train is schematically shown in Fig. 2). Note that the assumption of equal values of T_m, Δ_{ptp}, δ_{ptp} and A_0 is one of experimental and computational convenience and could be relaxed, if required. An m-train may be interpreted as a *single* pulse of special shape and special phase relations, and within certain limitations it can be made into a π-pulse with its own resonance parameters for frequency, amplitude, ptp-phase shift and ptp time delay. For such trains we will use the term "π-train", noting that its individual sub-pulses represent *fractional π-pulses.*

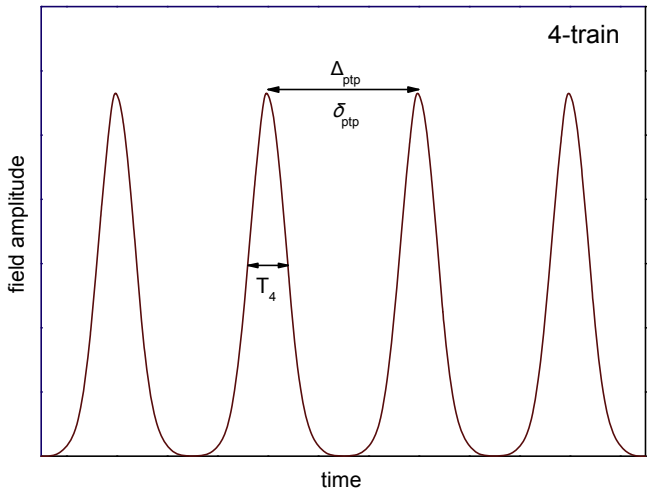

Fig. 2. Envelope function for a 4-train of gaussian sub-pulses with width (fwhh) T_4, pulse-to-pulse delay Δ_{ptp} and pulse-to-pulse phase shift δ_{ptp}. In all simulations T_4 = 2 ps (for m-trains $T_m = 8/m$ ps) and $\Delta_{ptp} > 20/m$ ps (with standard value $\Delta_{ptp} = 25/m$ ps).

The concept can be extended to multiple-order π trains. In analogy to $n\pi$-pulses ($n = 1,3,5,7,\ldots$) of successively higher fluence, which drive transitions sinusoidally in n Rabi half-cycles, $n\pi$-trains can be devised, again with n an odd integer. However, since each sub-pulse in an $n\pi$ m-train represents an $(n/m)\pi$-pulse, the population dynamics display a complex oscillatory evolution of target state population rather than stepwise accumulation of population. Illustrations of multiple-order π trains and some of their remarkable properties will be given in Section 4.3.

In any case, it is the crux of pulse-train control that an m-train possesses more parameters than are required to uniquely define a generalized π- or $n\pi$-pulse [13]. This means that the concept of a singular resonant π-pulse gives way to a "resonance locus" in (ω, A_0, δ_{ptp}, Δ_{ptp})-space characterizing an infinite set of resonant π-trains. In particular, as we will demonstrate in Section 4, the pair

of resonance parameters $\{\omega_r^{IF}, A_r\}$ of a gaussian pulse of given length, *i.e.* a point in the (ω, A_0)-plane, to an excellent approximation is replaced by a curve representing the projection of the resonance locus onto this plane, which we denote "resonance ridge". This increased flexibility allows making convenient choices for some of the parameters, and will strongly facilitate the control of parallel and branching processes.

3.3. The number of sub-pulses

The adiabaticity requirement [34], which demands that the pulse envelope must vary much more slowly than the oscillatory field, puts a constraint on the number of sub-pulses in a pulse train of given total width T_p, so that m cannot be made arbitrarily large. Furthermore, even before reaching this "few-cycle" limit for the sub-pulses, another important aspect comes into play. The narrowing of the sub-pulses associated with increasing m increases the width of the frequency distribution, so that the detuned intermediate levels will increasingly come into play. An m-train can lead to significant final rung-state population, as soon as T_m drops below a critical sub-pulse width T_c,

$$T_c = 2\pi/\mathrm{d}\varepsilon_{\min}, \tag{5}$$

where $\mathrm{d}\varepsilon_{\min}$ is the smallest of the individual rung detunings $\mathrm{d}\varepsilon_j$ defined in Eq. (2). In this case, the Fourier spectrum covers transition frequencies to at least one intermediate rung state $|j\rangle$, which could now be populated in a $(j-1)$-photon transition. The quantity T_c translates into a critical sub-pulse number m_c,

$$m_c = T_P/T_c, \tag{6}$$

which marks the transition between two regimes of m-trains.

Since $\mathrm{d}\varepsilon_{\min}$ depends on ω, upon sweeping the frequency the occurrence of accidental near-degeneracies of ω with ω_0^{Ij} for *single* specific levels j may lead to erratic behavior of m_c. For a "regular" anharmonic progression, *e.g.* a Morse progression, driven near $\omega = \omega_0^{IF}$ no such accidental degeneracies can arise, and m_c is a characteristic parameter of a system. Since intermediate state participation becomes noticeable well before reaching m_c, as a parameter characterizing the *effective* onset of rung-state intrusion we use the switch-over number

$$m_{sw} = 0.75 m_c, \tag{7}$$

where the choice of the factor 0.75 is purely empirical. We will use values of m_{sw} derived for $\omega = \omega_0^{IF}$ to define two regimes of "few" and "many" sub-pulses. Corresponding values of m_{sw} for our model systems are included in Table 1.

In m-regime I, defined by $m < m_{sw}$, final rung-state population will be negligible in general, and then the situation for π-trains will be comparable to that of simple π-pulses, except that the sinusoidal increase (decrease) of P_F (P_I) will be replaced by a stepwise sinusoidal one. Rung-state population will at most be a transient phenomenon. In m-regime II, $m > m_{sw}$, and participation of rung states, which may become sizable for certain train parameters, will be the rule. However, this state of affairs need not imply *final* rung-state population, since A_0, Δ_{ptp} and δ_{ptp} can be used as adjustable parameters maximizing P_F.

3.4. Few sub-pulses, m-regime I

We will now develop the conditions required for complete accumulation of population in the target state by a pulse train, *i.e.* $P_F \to 1$. We start by considering a k-photon excitation at $\omega = \omega_0^{IF}$. In a zero-order picture the time evolution of the target state remains in phase with the field oscillations for all times, provided the δ_{ptp} are adjusted such that

$$\delta_{ptp} = \delta_{ptp}^{\nu} = \nu \cdot 2\pi/k, \quad \nu \text{ any integer}. \tag{8}$$

There is no dependence on Δ_{ptp}, which thus may be chosen arbitrarily, *e.g.* as small as possible compatible with the requirement of non-overlapping sub-pulses, or so as to satisfy experimental demands. Although there may be perturbations introduced by Fourier components from the pulse envelopes, we find that these can be neglected in all our examples.

From Eq. (8) it follows that in $[0,2\pi]$ there are k different, equally spaced "constructive" values δ_{ptp}^{ν}. In a zero-order picture, for each of these values and for arbitrary Δ_{ptp} the fractional π-pulses forming the train will combine to an overall π-pulse, *i.e.* a π-train. Importantly, by choosing a suitable ν, one can discriminate degenerate transitions of different photonicity and hence has control over parallel or branching processes.

For realistic systems the zero-order assumptions are not strictly fulfilled. First, in NLSs the area theorem [11] is not obeyed [12,13,34], especially in mp processes, sometimes not even approximately. Hence the area under the envelope of differently shaped "π-pulses" is not invariant, and A_r will not be the optimal field amplitude. Also, in the same way as for simple π-pulses, where $\gamma^{IF} = 0$ holds only in the limit of vanishing field, an m-train tuned to ω_0^{IF} and δ_{ptp}^{ν}, will only be an *approximate* π-train.

Since an m-train has more tunable parameters than are required to define a generalized π-pulse, we can proceed from zero-order π-trains to "proper" ones by readjusting the parameter set $\{\omega, A_0, \Delta_{ptp}, \delta_{ptp}\}$. As discussed below, an additional relation links these parameters, so that three variables are available to meet the condition for a generalized π-pulse. Instead of a unique resonant π-pulse, a set of π-trains will exist forming a "resonance locus" in parameter space, where within limits two of the parameters can be chosen freely. In Section 4 we will explore resonance loci for our model systems by numerical means. A full understanding of their properties requires an in-depth theoretical analysis. Sidestepping this for the present paper, we provide only a brief phenomenological discussion.

It is particularly instructive to take ω as a parameter to be fixed in advance, and to distinguish the cases $\omega = \omega_0^{IF}$ and $\omega \neq \omega_0^{IF}$. For trains in m-regime I tuned to $\omega = \omega_0^{IF}$, Δ_{ptp} is arbitrary and is not available for optimization. Hence Δ_{ptp} can be chosen freely (but see below for some additional observations). The remaining parameters A_0 and δ_{ptp} can be adjusted to define a set of π-trains differing only in δ_{ptp}, as implied by the periodicity shown in Eq. (8). Upon optimization, δ_{ptp} will deviate from the zero-order estimates in Eq. (8), so that

$$\delta_{ptp} = \delta_{ptp}^{\nu} + \Delta\delta_{ptp} \quad \nu \text{ any integer}. \tag{9}$$

For a k-photon process, in $[0,2\pi]$ there are k equally spaced constructive values of δ_{ptp}. For a given m, the optimized values of A_0 and δ_{ptp} together with ω_0^{IF} and any convenient value of Δ_{ptp} define π-trains. We note that even in m-regime I rung contributions are not *strictly* zero. If required, the remaining dependence on Δ_{ptp}, usually negligible by construction, could be used to maximize P_F.

In contrast to the zero-detuning case treated above, for an m-train detuned from ω_0^{IF} the choice of Δ_{ptp} is not arbitrary. Constructive interference between the sub-pulse contributions maximizing P_F occurs only for certain parameter triples $\{A_0, \delta_{ptp}, \Delta_{ptp}\}$. Apart from its general m-dependence, for all practical purposes A_0 depends only on ω, while for any given δ_{ptp}, the associated value of Δ_{ptp} recurs with period T_δ,

$$T_\delta = 2\pi/k\hbar|\omega - \omega_0^{IF}| \tag{10}$$

the phase recurrence time. Hence with ω fixed and A_0 as determined, there exists an infinite set of pairs $\{\delta_{ptp}, \Delta_{ptp}\}$ fulfilling the conditions for a π-train. Again δ_{ptp} also obeys the k-photon periodicity rule of Eq. (8). In praxis a convenient value of either δ_{ptp} or Δ_{ptp}

can be pre-selected. The first method, with the possibility of using phase-locked trains *e.g.* with $\delta_{ptp} = 0$ or π [35], may be useful in the laboratory. In this paper, for better comparability of different π-trains we will mainly make use of a pre-selected value for Δ_{ptp}. Note since Eq. (10) does not hold for overlapping sub-pulses, an accurate explicit equation for δ_{ptp} connecting to $\Delta_{ptp} = 0$ is not readily available. Suitable values may be found by numerical optimization, from which other π-pulse parameters may be derived using Eqs. (8) and (10). Predictably, apart from their m-dependence the constructive parameter triples $\{A_0, \delta_{ptp}, \Delta_{ptp}\}$ also depend on ω, and in Section 4.3 we will show the interesting patterns arising.

So far we have assumed there is no accidental near-degeneracy of ω with one of the rung transition frequencies ω_0^{Ij}. For $\omega \neq \omega_0^{IF}$ such a situation may occur, and then in order to avoid final population of level $|j\rangle$, methods suitable for m-regime II, as elaborated below, must be used. A pair $\{\delta_{ptp}, \Delta_{ptp}\}$ has to be found that takes care of Eq. (10) *and* minimizes the rung-state populations P_j.

3.5. Many sub-pulses, m-regime II

In addition to the optimization of A_m and δ_{ptp}, the design of π-trains in m-regime II requires adjustment of Δ_{ptp} in order to avoid final population of rung states. At any ω, except at one of the zero-order frequencies ω_0^{Ij} relating to the $|I\rangle \rightarrow |j\rangle$ (j-1)-photon transition, the rung states $|j\rangle$ are subject to phase recurrence, with phase recurrence time

$$T_j = 2\pi/(j-1)\hbar|\omega - \omega_0^{Ij}|. \tag{11}$$

Again, as for T_δ in Eq. (10), accurate explicit equations for the T_j connecting to $\Delta_{ptp} = 0$ are not readily derived. Furthermore, additional oscillations may be superimposed due to coupling among different transitions.

Successful population transfer to the target state requires identifying parameter quadruples $\{\omega, A_0, \delta_{ptp}, \Delta_{ptp}\}$ such that $|F\rangle$ behaves constructively, while simultaneously all relevant rung states interfere destructively. Note in this context that *rung-state participation* may also become manifest as finial *initial state population* of varying degree, if the train is not "π" with respect to the rung transitions (which is likely).

The requirement to simultaneously fix several parameters with different periodicities means the optimization has to be screened over extended ranges of Δ_{ptp}. This implies optimization in a huge rugged parameter space and the possibility of trading in perturbations from rotation or spontaneous emission. The task will be weakly alleviated by keeping to ω_0^{IF}, so that δ_{ptp} can be fixed at one of its constructive values from Eq. (9), and P_F need not be monitored for its phase recurrence.

3.6. Embedded progressions

We conclude this section addressing the question under which conditions ladder climbing within an extended anharmonic progression can be described by the minimal system, *i.e.* an $(n+1)$LS for an n-photon excitation, and how "outer" rung states would affect the train-driven dynamics. Note in order to arrive at general conclusions, in the following we disregard accidental degeneracies of ω with an outer rung transition, assuming *e.g.* that ω is chosen to lie in the vicinity of ω_0^{IF}.

In m-regime I, in a regular anharmonic progression no changes with respect to the unembedded system are expected, because the outer rung states are more strongly detuned than the inner ones, and hence will not be covered by the spectral width of the train. Under such conditions the embedded system can be reduced to a minimal one involving only the rungs from $|I\rangle$ to $|F\rangle$. This is in strong contrast to harmonic progressions, where an equivalent of m-regime I does not exist, and a cutoff of outer states causes artificial accumulation of population in the lowest and/or uppermost levels.

In m-regime II, participation of outer states will naturally arise as soon as they get into the reach of the frequency spread, and an obvious extension of Eq. (10) holds for these states. For regular anharmonic progressions, again due to the larger detuning of outer states, this will happen well inside m-regime II, while as long as m is not too large, differences to the unembedded systems will remain moderate. In Section 4, these features will be demonstrated for the embedded 3LS.

4. Results

All simulations reported in this section are based on numerical integration of the Schrödinger equation (for technical details see Ref. 36). The gaussian pulses are considered to be negligibly weak when the envelope drops to about 0.1% of the maximum field strength, corresponding to an integration interval of 3.125 T_p (*i.e.* 25 ps for our standard pulse length $T_p = 8$ ps). As reference values for pulse-train control, parameters for simple gaussian π-pulses are collected in Table 2. Selected higher-order π-pulses are included in some of the following figures.

The main body of this section is made up by our results for π- and $n\pi$-trains obtained numerically following the prescriptions in Sections 3.4 and 3.5. As a pragmatic definition of π-trains we use the criterion $P_I < 10^{-3}$, with the additional goal to maximize P_F, possibly beyond 0.99. We concentrate on the 2-photon transition in the embedded 3LS and the 5-photon transition in the 6LS, which cover all aspects of interest and show the full variation from near-ideal to complex behavior. The 4LS and 5LS are intermediate in all aspects; selected results are included in Table 2.

We recall that all results relate to m-trains with equal total sub-pulse length, such that $mT_m = 8$ ps. The train *duration* may vary due to the variable ptp time delay, although whenever there is a choice, for better comparability we use $\Delta_{ptp} = 25/m$ ps, corresponding to a duration of 25 ps from effective "field on" to effective "field off", ignoring current experimental limitations which would call for distinctly longer values of Δ_{ptp}.

4.1. Pulse trains at ω_0^{IF}

Parameters for π-trains tuned to $\omega = \omega_0^{IF}$ as obtained in our optimizations are collected in Table 2. Near-ideal behavior is found in m-regime I, most cleanly for 2-photon excitation in the 3LSs. In the

Table 2
Properties of π-trains at $\omega = \omega_0^{IF}$

	m[a]	3LS	emb. 3LS	4LS	5LS	6LS
A_r[b]	1	.0002903	.0002893	.0008299	.001733	.003086
A_0[c]	4	.0002875	.0002862	.0008230	.001728	.003095
	8	.0002743	.0002728	.0008069	.001708	.003055
	16	–[g]	.0002840	.0006920	.001582	.002940
	24	–[f]	–[f]	–[f]	–[f]	.002586
γ^{IFd}	1	.07	.0001	.40	1.26	2.94
$\Delta\delta_{ptp}$[e]	4	.0009	−.000003	.0048	.0145	.0333
	8	.0004	−.00003	.0022	.0068	.0158
	16	–[g]	–[g]	–[g]	.0028	.0072

[a] Number of sub-pulses.
[b] Resonance amplitude (field strength in a.u.) for gaussian π-pulse with $T_p = 8$ ps.
[c] Resonance amplitude (field strength in a.u.) for π-train.
[d] Bloch–Siegert shift (in 10^{-6} a.u.) for gaussian π-pulse with $T_p = 8$ ps.
[e] ptp-phase shift (in units of 2π) for π-train.
[f] Not calculated.
[g] In m-regime II; pronounced Δ_{ptp} dependence.

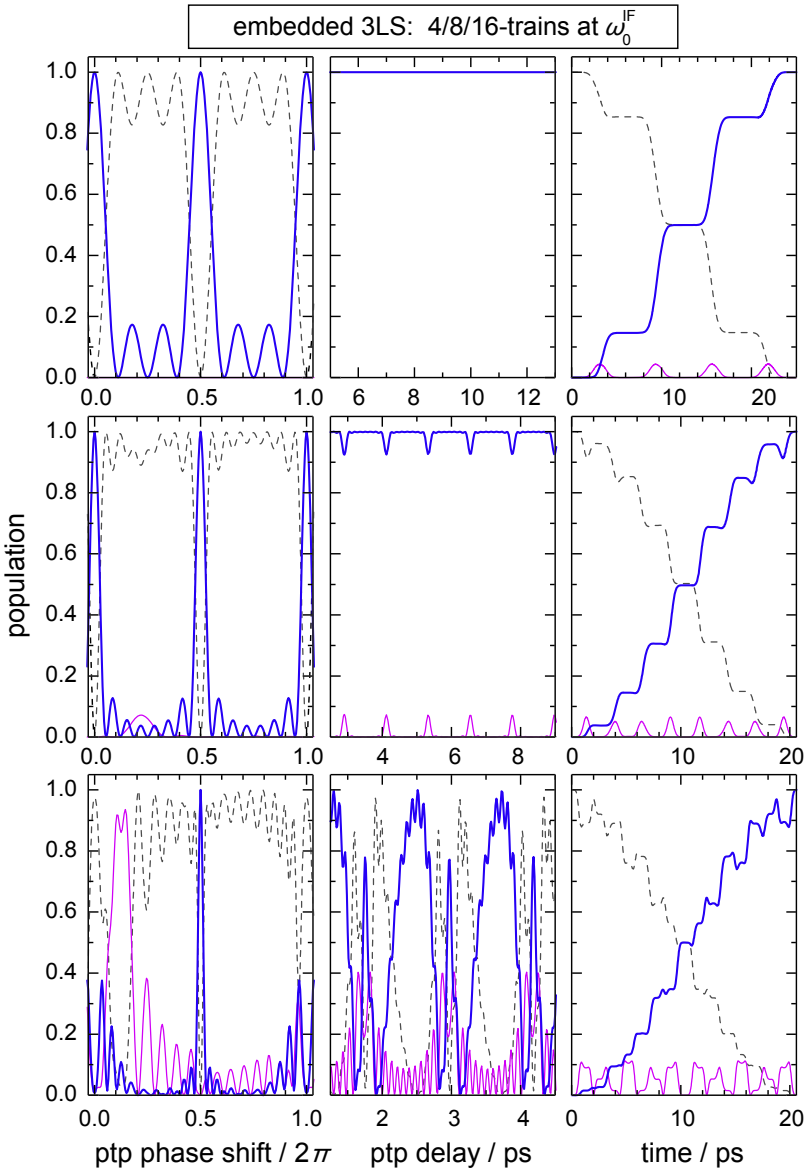

Fig. 3. Results for the embedded 3-level system driven by m-trains at the zero-order resonance frequency ω_0^{IF} and the respective resonance field amplitude A_0 (values shown in Table 1). Top row: sub-pulse number $m = 4$; middle row: $m = 8$; bottom row: $m = 16$. Left column: phase portraits (δ_{ptp}-dependence) at optimum Δ_{ptp}; middle column: Δ_{ptp}-dependence at $\delta_{ptp} = 0$. Right column: population dynamics for π-trains. Bold full lines (online blue): target state population P_F; gray broken lines: initial state population P_I; thin full lines (online magenta): rung population P_2.

top row of Fig. 3 we show results obtained for the embedded 3LS driven by 4-trains at central frequency ω_0^{IF}, noting that the results are extremely close to those for the pure (minimal) 3LS, as anticipated in Section 3.6.

The three top panels, showing in turn the phase portrait and the Δ_{ptp} dependence for 4-trains, and the population dynamics for a π-train, demonstrate, respectively, the constructive behavior near $\delta_{ptp} = 0$ and π, in agreement with Eq. (8), the independence of the control parameters from Δ_{ptp}, and the accumulation of population in the target state by stepwise sinusoidal evolution of P_F. As in simple π-pulse excitation, there is some transient rung-state population. Other deviations from ideal behavior, although present, are insignificant, and target state populations close to 100% are obtained with the zero-order parameters, independent of Δ_{ptp}.

More pronounced deviations from zero-order behavior become gradually apparent for the 8- and 16-train results in the middle and bottom row panels of Fig. 3. Here the conditions correspond to m-regime II, so that Δ_{ptp} must be monitored for rung-state participation. For $m = 8$, just inside m-regime II, the perturbations are weak and readily handled, while for 16-trains we are already faced with an involved optimization problem, accompanied by a strong degradation of the robustness of the method. Furthermore the population dynamics attain signs of irregularities, indicating that some of the intrinsic deviations from ideality can be, and actually are, compensated by elements of brute-force parameter optimization.

Fig. 4 is equivalent to Fig. 3, but for 5-photon excitation in the 6LS. Since $m_{sw} = 20$, both $m = 8$ and 16 are in m-regime I. We still observe near-ideal behavior, the main difference to the 2-photon transition being the more pronounced transitional rung-state participation. This behavior, though, is not specific to train-driven dynamics, and is also found for simple π-pulses. In m-regime II ($m = 24$ is chosen in our example, noting that the maximum number of sub-pulses due the onset of the regime of few-cycle pulses is about 50), matters become more complicated, as there are now four rung states, all with their own phase recurrence times. The

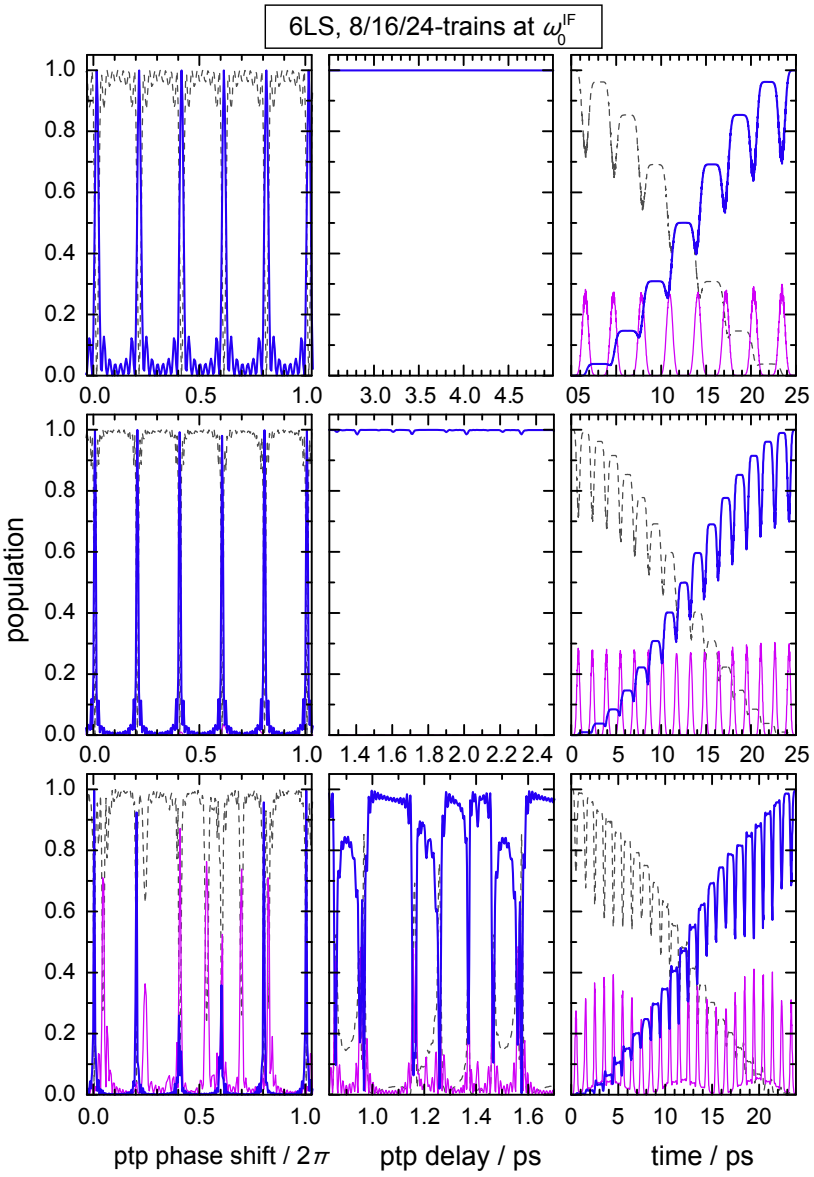

Fig. 4. Results for the 6-level system driven by m-trains at the zero-order resonance frequency ω_0^{IF}. Plot layout and conventions are as in Fig. 3; the rung population refers to the sum of all rung states.

appearance of the phase portrait and the delay dependence are more congested and less symmetric than in the 3LS, indicating fairly involved parameter optimization. For Morse progressions, at ω_0^{IF} degeneracies arise for the rung detunings, which give rise to simplifications in the phase recurrence patterns. For perturbed progressions, as in realistic molecular systems, such commensurability-related reduction in complexity will be absent, and the parameter search may be even more involved.

Altogether, Figs. 3 and 4 together with the data in Table 2 illustrate the following observations concerning the effects of increasing the number of sub-pulses, which all hold across both m-regimes.

(1) Specificity and selectivity of train-driven population transfer increase with m. Thus the phase portraits in the left hand panels of Fig. 3 show the narrowing of the peaks of constructive interference, with widths decreasing as m^{-1}. This behavior parallels many well-known interference phenomena. Obviously the increase in selectivity is traded in by a reduction of the robustness. Although in the present context of simple ladder climbing excitations there is no need to go for the increased selectivity, this may become an important issue in the separation of competing processes.

(2) For π-trains run at ω_0^{IF}, the shift $\Delta\delta_{ptp}$ given in Eq. (9), which specifies the deviation of δ_{ptp} from the zero-order values δ_r^v (*i.e.* 0 and π for the 2-photon process in the 3LS), decreases approximately as m^{-1}. It thus tends to zero in the limit $m \to \infty$ (which obviously can only be taken naïvely). Still this behavior is of pragmatic interest, as for the case of large sub-pulse numbers it indicates the possibility of fixing δ_{ptp} *ab initio* at its zero-order value, or at least it allows a considerable reduction of the tuning range. The entries shown in Table 2 demonstrate that the trends in the $\Delta\delta_{ptp}$ reproduce those in γ_{IF} for the corresponding gaussian π-pulses.

(3) Due to the failure of the area theorem, splitting a gaussian π-pulse into an m-train requires re-adjustment of A_0 (performed in conjunction with adjusting the remaining parameters). The optimized values decrease with increasing m. This behavior becomes more pronounced for more extended ladders.

4.2. Detuning: pulse trains at $\omega \neq \omega_0^{IF}$

Using trains with ω detuned from ω_0^{IF} requires simultaneous optimization of A_0, δ_{ptp} *and* Δ_{ptp}, even in m-regime I. Representative results are shown in Figs. 5 and 6, which are the "detuned" counterparts of Figs. 3 and 4. The specific frequencies used in our examples, denoted ω_0^{IB}, have no particular meaning in the context of this paper, but are reference frequencies for intruder state control treated elsewhere.

A significant qualitative difference to the zero-detuning case occurs for the Δ_{ptp}–dependence. From Eq. (10), in both m-regimes there are successive "constructive" Δ_{ptp} windows separated by T_δ. There are also some remarkable effects on the population dynamics, which will be discussed in Section 4.3. In all other respects the mechanisms of train-induced population transfer are remarkably robust against variations in ω. For all systems, the resulting phase portraits are shifted versions of those for ω_0^{IF} (with small deviations in m-regime II as discussed below). Across both ranges, the "constructive peaks" in the phase portraits become narrower with increasing m, the widths decreasing as m^{-1}. The changes and additional features seen in m-regime II, which do not affect the properties of the π-trains themselves, derive from the different detunings of the rung states. Consequently the patterns are affected mainly by the different spacing of the individual recurrences, and by the differences in strength and fractional π character of the rung transitions.

Contour plots of P_F in the (Δ_{ptp}, δ_{ptp})-plane are shown in Fig. 7 for various values of ω (here demonstrated for 4-trains in the embedded 3LS, well inside m-regime I). The recurrences in Δ_{ptp} and the periodicities in δ_{ptp} are clearly apparent in these 2D plots, which also illustrate the dependence of the phase recurrence on the detuning. The slope of the ridges is related, *via* Eq. (8), to the detuning, the sign of the slope indicating the direction of detuning. The plots also illustrate how the detuning affects the robustness, switching from completely robust with respect to Δ_{ptp} to mildly robust against variations in δ_{ptp}.

Since A_0 is constant for π-trains at a given ω, the ridges of maximum P_F remain at constant height ($\approx$1). An important point concerns the variation of A_0 as function of ω. This includes the questions about the minimum value of A_0, denoting the π-train of lowest fluence, *i.e.* the most efficient, "optimum" resonant driving field, and about the range of ω-values permitting resonant

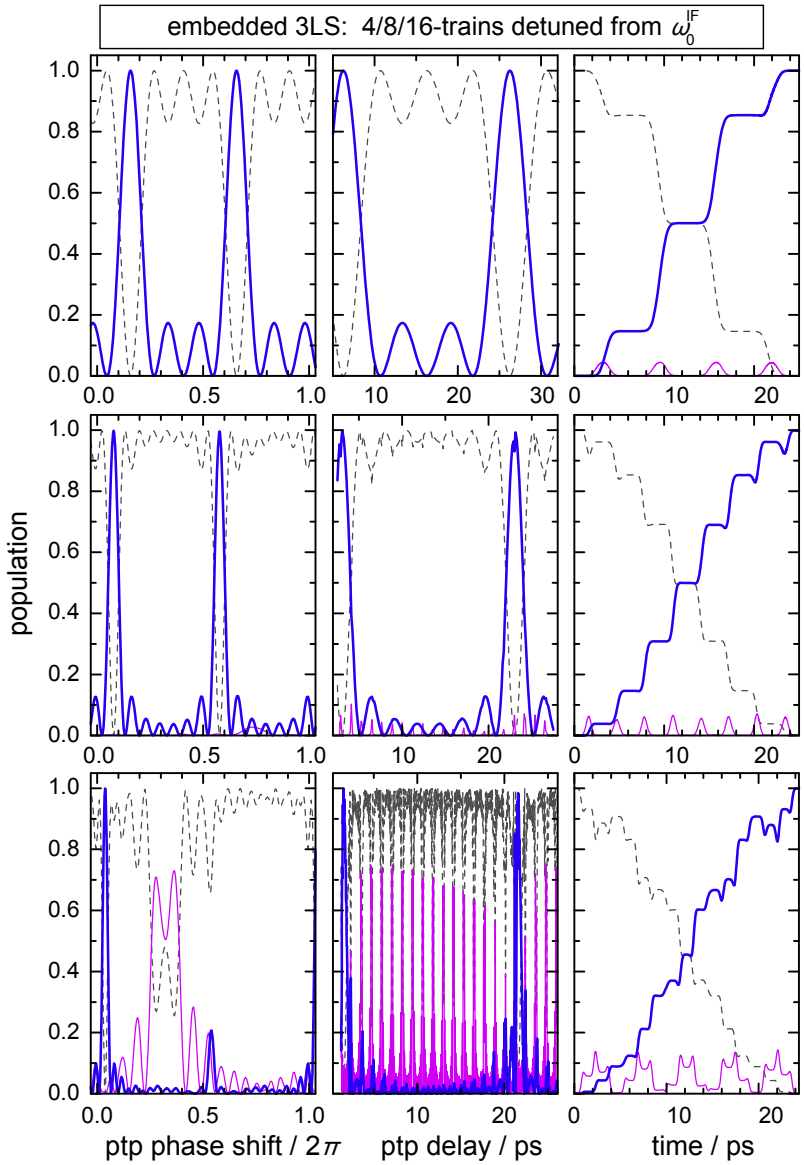

Fig. 5. Results for the embedded 3-level system driven by m-trains detuned from ω_0^{IF} by -3.8×10^{-5} a.u. (see text). Plot layout and conventions are as in Fig. 3.

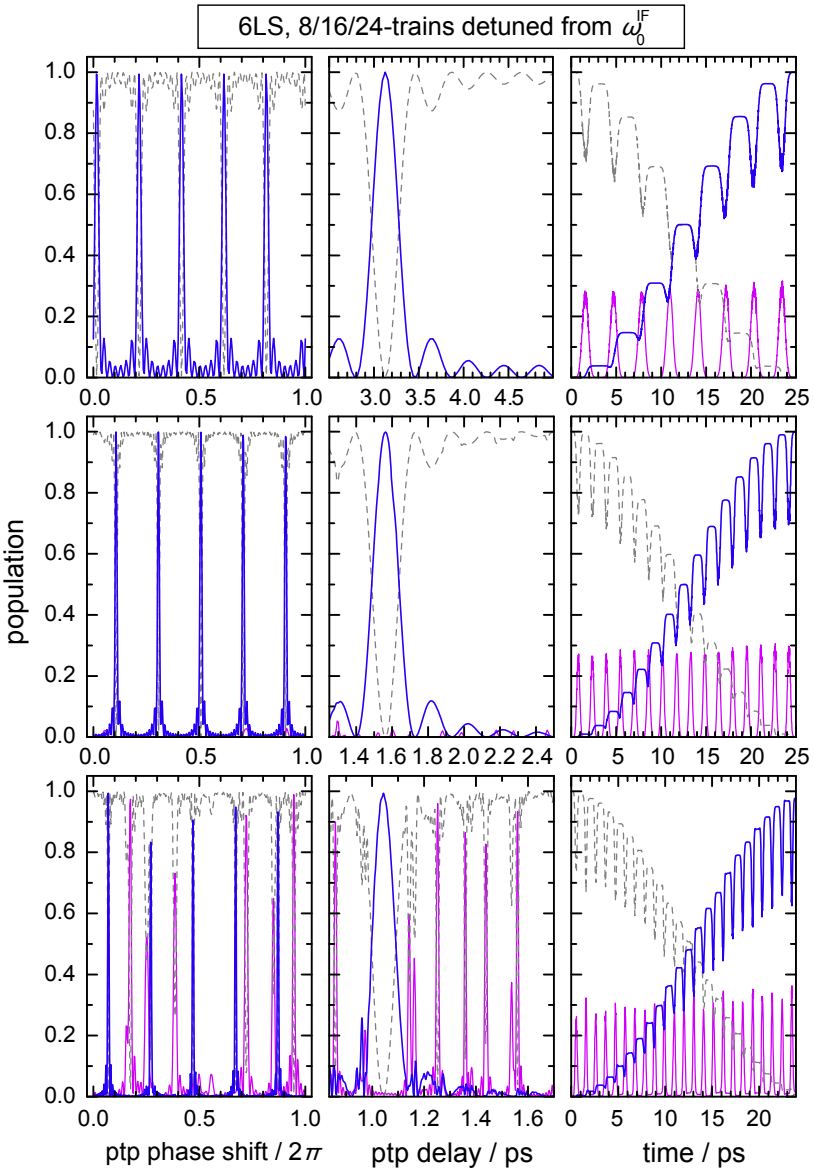

Fig. 6. Results for the 6-level system driven by m-trains detuned from the zero-order resonance frequency by -1×10^{-4} a.u. (see text). Plot layout and conventions are as in Fig. 3; the rung population refers to the sum of all rung states.

excitation. These properties, which are best visualized by the projection of the resonance loci onto the (ω,A_0)-plane, and the variation of the population dynamics with ω, are closely linked to the existence and behavior of multiple-order π trains. In the following subsection we will cover these topics jointly.

4.3. Resonance ridges and multiple-order π trains

In Fig. 8 we show projections of resonance loci for the embedded 3LS and the 6LS onto the (ω,A_0) plane, covering the first few (odd) $n\pi$-trains. We refer to the resulting curves as *resonance ridges*. The most striking feature is the emergence of extended closed-loop curves representing conditions for complete resonant population transfer. For reasons of mutual comparability we use fixed values of Δ_{ptp} (8.5 ps for 2-trains, 4.25 ps for 4-trains, and 2.125 ps for 8-trains) and accordingly adjusted values of δ_{ptp}; in view of the regular phase recurrences this represents no loss of generality. We also keep the trains in m-regime I, where these conditions can be maintained.

Comprehensive information on the full 4-dimensional resonance loci is obtained by combining the resonance ridges with contour plots in the $(\Delta_{ptp},\delta_{ptp})$-plane. The combination of Figs. 8a and 7 provides a visualization of the resonance locus for 4-train excitation in the embedded 3LS; the respective subspaces are mutually connected at the points marked in the plots. Lines superimposed on the contour plots indicate the continuation of the resonance ridge into the $(\Delta_{ptp},\delta_{ptp})$-subspace, hence these lines represent projections of the resonance loci onto the $(\Delta_{ptp},\delta_{ptp})$-plane. In general, in m-regime I there is an infinite manifold of $n\pi$-trains associated with each point of a resonance ridge. Note however that in frequency ranges with rung intrusion P_F may not reach unity. In m-regime II the topography of the resonance loci is far more complicated and rugged, and we do not further investigate this regime.

The variability of the parameters on the resonance loci puts π-trains in strong contrast to simple $n\pi$-pulses. In Fig. 8, the latter are indicated as open circles; the displacements from the curves representing $n\pi$-trains show the extent of failure of the area

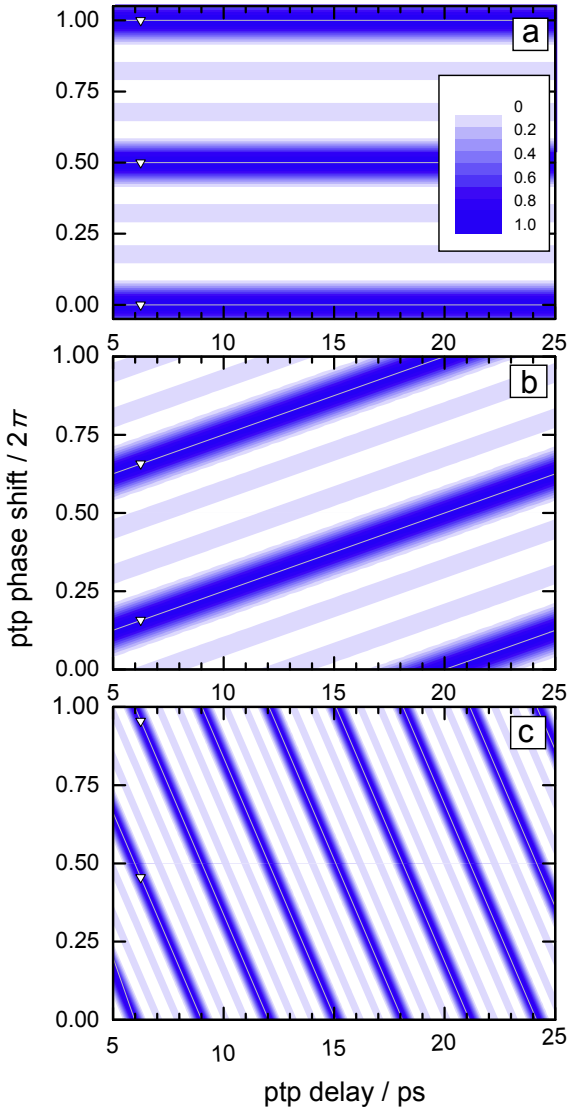

Fig. 7. Contour plots in the $(\Delta_{ptp}, \delta_{ptp})$-plane for the final target population P_F in the embedded 3-level system driven by 4-trains. Panels (a–c) are for different frequencies ω. In all cases, the field amplitudes are the optimized π-train values. The points indicated by triangles (online blue) correspond to the positions on the resonance ridge indicated by analogous marks in the upper panel of Fig. 8.

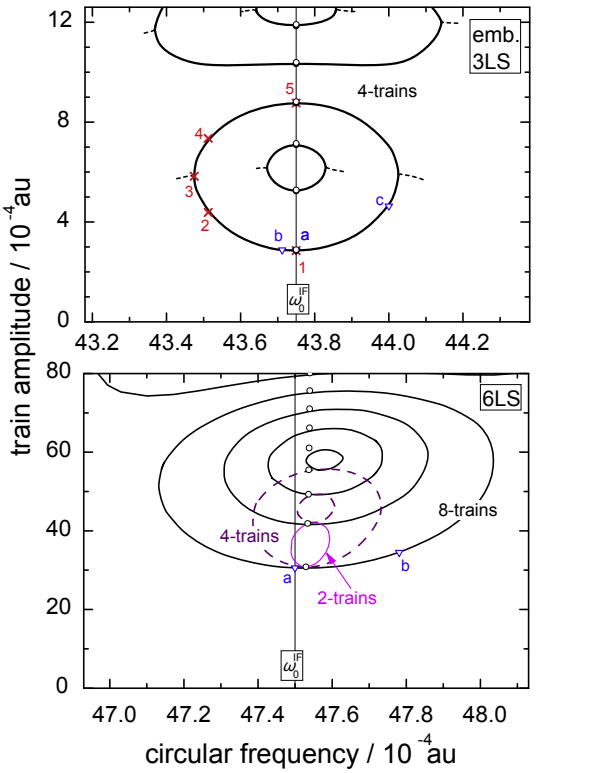

Fig. 8. Resonance ridges for $n\pi$-trains in the embedded 3-level system (top panel) and the 6-level system (bottom panel). Open circles denote gaussian $n\pi$-pulses ($n = 1,3,5,7,9,11,13$). In the top panel, triangles (online blue) marked a, b and c indicate parameter pairs relating to Fig. 7a–c, and crosses (online red) marked 1–5 indicate parameter pairs relating Fig. 11. In the bottom panel, triangles (online blue) marked a and b indicate parameter pairs relating to Fig. 9a and b, and resonance ridges for different sub-pulse numbers m are shown as identified in the labels: thin full line (online magenta): $m = 2$; broken lines (online purple): $m = 4$; bold black line: $m = 8$.

theorem. Around these points P_F declines in Lorentzian fashion. Along the resonance ridges a similar decline occurs in direction orthogonal to the curve, suggesting the notion of a resonance ridge.

The minimum of A_0 on the lowest resonance ridge specifies the π-train of minimum fluence. We denote its value A_{mf} and the corresponding frequency ω_{mf}: In the embedded 3LS, ω_{mf} is close to ω_0^{IF}, and the shift (about 10^{-7} a.u. ≈ 0.01 cm^{-1}) cannot be discerned on the scale of Fig. 8a. In fact the numerical determination of the "true" minimum position ω_{mf} is irrelevant for practical purposes. In contrast, in the 6LS ω_{mf}, and along with it the entire closed-loop ridge structure, are more distinctly shifted (by about 1 cm^{-1}) from ω_0^{IF}. The difference reflects much higher field intensities required for the 5-photon transition than for the 2-photon transition, and is also present on the level of simple π-pulses. In fact the values of ω_r^{IF} and ω_{mf} are close for all systems treated. In conclusion, due to the variability of π-trains, the train-analogue of the Bloch–Siegert shift has different manifestations, such as a pure extra ptp-phase shift in the special case $\omega = \omega_0^{IF}$, but also an interpretation as frequency shift from ω_0^{IF} to ω_{mf} that characterizes the *most efficient* way of train-induced resonant excitation.

The full ensemble of multiple π-trains accounts for a remarkable robustness of population transfer in m-regime I. The extent to which the resonance loci fill the parameter space is illustrated in Fig. 9. For the example of 8-train 5-photon excitation in the 6LS, we show that the resonance loci fill extended stretches of the (A_0, δ_{ptp}) plane fairly densely. This behavior persists for a range of frequencies: compare the two panels taken at different values of ω. Furthermore, Δ_{ptp} is kept at 3.125 ps in both example, however some sensitivity with respect to Δ_{ptp} must be expected due to phase recurrence. In any case, sizable pulse-train induced population transfer occurs over extended regions of the parameter space.

Since due to its robustness against the ptp time delay, ω_0^{IF} is a useful choice for control purposes, we next consider the sequence of $n\pi$-trains at the zero-order transition frequency. For the embedded 3LS the usual properties known from simple $n\pi$-pulses are recovered, with increasingly complex piecewise sinusoidal population dynamics; examples are included in Fig. 10. If an analogous analysis is performed for the 6LS, then as seen in Fig. 8b a gap appears, with the 7π- and 9π-trains apparently missing. These irregularities are caused by the frequency shift to ω_{mf}. Repeating the exercise at ω_{mf}, the completeness of the $n\pi$-trains is re-established.

We conclude this section with a phenomenological discussion on the origins of the closed-loop form of the resonance ridges. A symmetry principle operates such that the closed curves connect $n\pi$-trains with identical intermediate populations P_I and P_F after each sub-pulse. This means that for an m-train the 1π and the $(2m\text{-}1)\pi$-train interact, or more generally, the (odd) $k\pi$- and $l\pi$ trains with $k + l = 2m$. Thus for 4-trains the 1π-and 7π-trains both have intermediate populations 1/4, 1/2, 3/4, 1, and similarly 3π

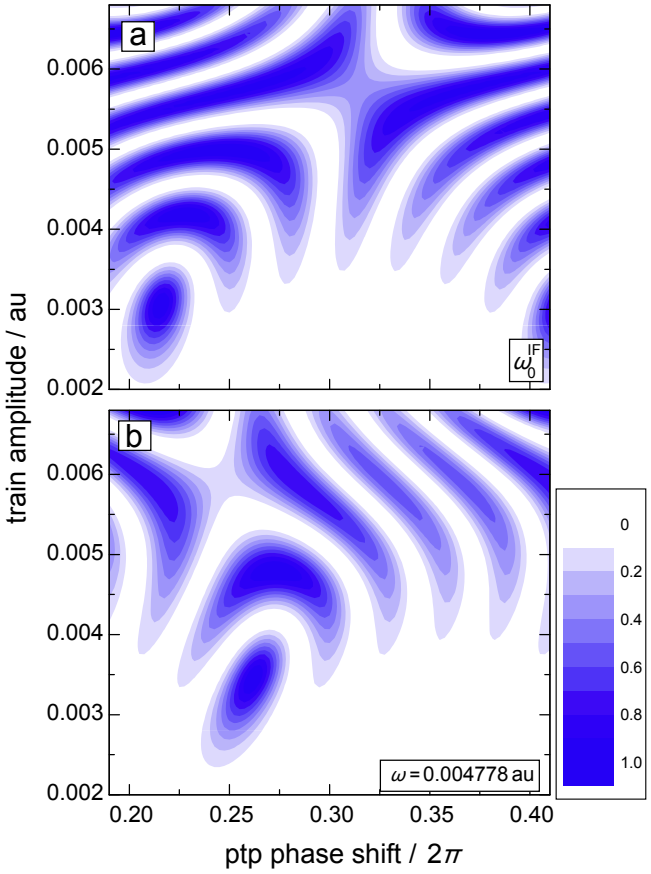

Fig. 9. Contour plots in the (δ_{ptp}, ω)-plane for the final target population P_F in the 6-level system driven by 8-trains with ptp time delay $\Delta_{ptp} = 3.125$ ps. Panels (a) and (b) are for different frequencies ω corresponding to the points on the lowest resonance ridge (1π-trains) marked a and b in Fig. 8b.

and 5π trains show the sequence 3/4, 1/2, 1/4, 1. We did not investigate the continuation to π-trains beyond order $2m - 1$.

Fig. 8b also illustrates how the frequency range covered by the loops increases with m. For the lowest branch, the m-dependence and the dependence of A_0 on the detuning qualitatively agree with the trends of the RWA results for 2LSs as obtained by Vitanov and Knight [1], except that the detuning should be considered relative to ω_r^{IF} rather than to ω_0^{IF}. Note the results are not directly comparable, since in Ref. 1 the authors consider the m-dependence at constant sub-pulse width.

It is instructive to follow the change in the population dynamics along a resonance ridge. The dynamics transform smoothly, *e.g.* from one to seven Rabi half-cycles in the example shown in Fig. 11. Well away from ω_{mf} the population dynamics do not allow to unequivocally identify the order n of the "$n\pi$-train".

5. Conclusions

If m-trains consisting of fractional π-pulses with suitably adjusted ptp phase shifts and ptp time delays are substituted for simply-shaped π-pulses, additional tuning parameters become available for the control of state-specific ladder climbing mp transitions. Even under the restriction to equal sub-pulse properties, the additional tunable parameters Δ_{ptp} and δ_{ptp} together with the handle on m, the number of sub-pulses, open up an extended control space.

At fixed overall pulse width, to each m there are infinite sets of π- and multiple-π trains. They occupy resonance loci in parameter space. Multiple-π trains of different order interact and couple according to a symmetry law imposed by m. In m-regime I, they form well structured extended 4-dimensional objects, which project onto the (ω, A_0)-plane as manifolds of concentric ellipsoidal curves. We term these closed curves resonance ridges.

The fact the frequency can be tuned freely over a certain range and is not restricted to the singular resonance frequency associated with simply-shaped π-pulses can be a formidable asset in the

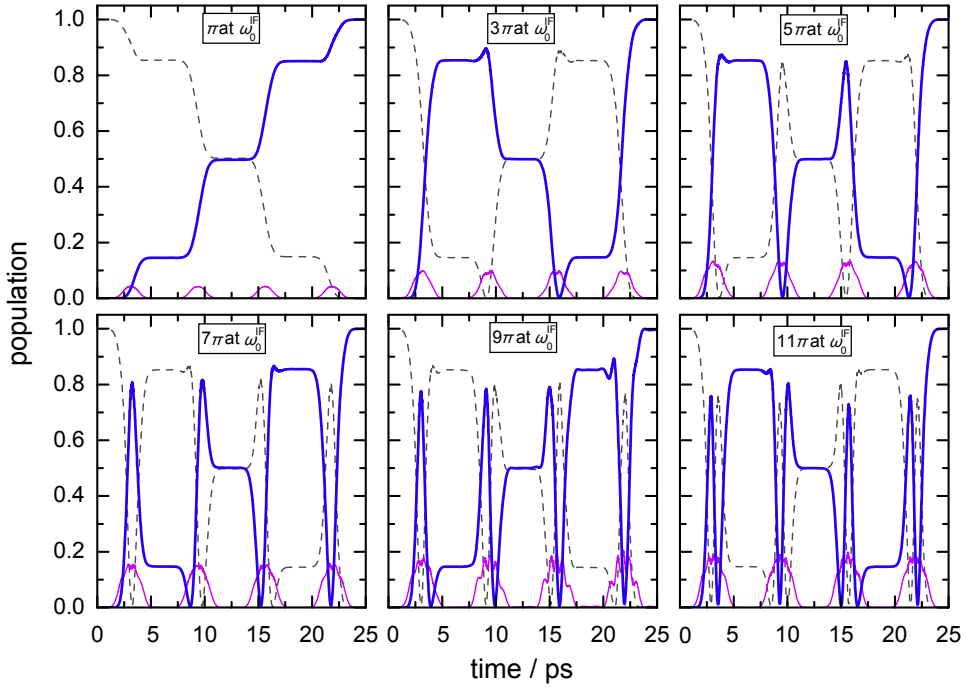

Fig. 10. Population dynamics in the embedded 3-level system for $n\pi$-trains at the zero-order resonance frequency ω_0^{IF}. Plot conventions are as in Fig. 3. For $n \geq 5$, small transient outer rung-state populations (<0.04) are not shown in the plot.

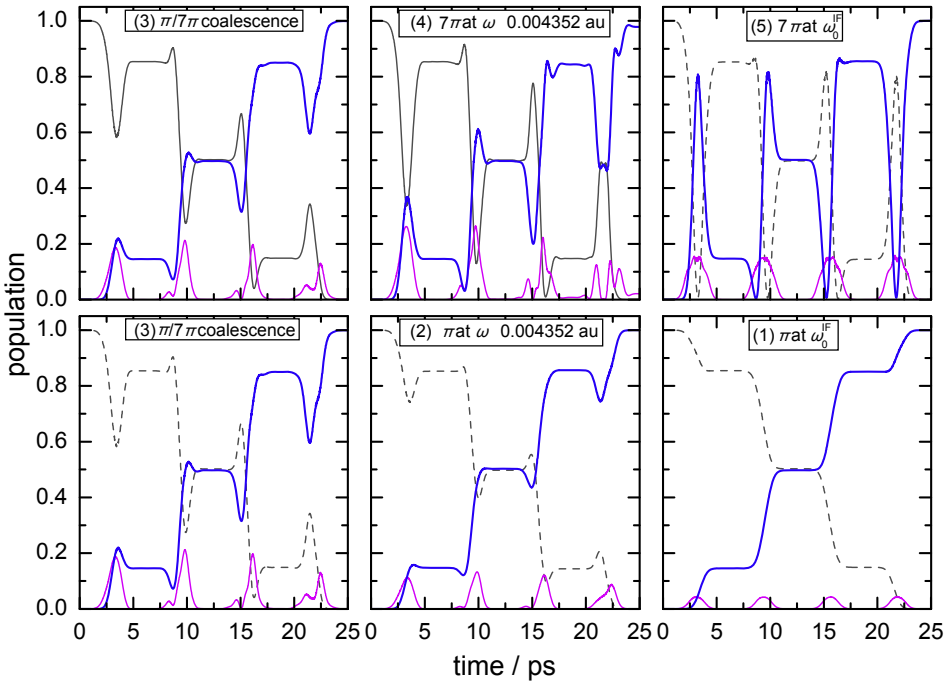

Fig. 11. Population dynamics in the embedded 3-level system along the resonance ridge connecting the 1π- and 7π-trains. The panels (1)–(5) correspond to the points on the resonance ridge marked 1–5 in the top panel of Fig. 8. Panel (3) is repeated for improved layout. Plot conventions are as in Fig. 3.

control of background state population or of competing parallel or branching transitions. It strongly enhances the possibilities offered by the zero-order properties of Δ_{ptp} and δ_{ptp}, which are, respectively, sensitive to the photonicity of the transitions and the level detunings. In *m*-regime I, zero-order estimates for the tuning parameters will at least facilitate the optimization, and for mp transitions of low photonicity, which do not show sizable *transient* rung-state population, these estimates can be applied more or less directly.

Complications arise upon entering *m*-regime II, where the short and hence spectrally broad sub-pulses can populate even strongly detuned rung states. The necessity to control all these states simultaneously turns the extended resonance loci into scattered stretches in parameter space, and closed-loop self-learning algorithms, similar to those used in optimal control [37–39], may be useful for an efficient optimization. Although reverting to *m*-regime II looks unfavourable in view of these complications, this option may be of practical interest for the control of parallel, competing or entangled transitions, since an increase in *m* increases the specificity of the transitions and may thus help to separate such processes.

Elsewhere (M. Seidl, M. Etinski, Ch. Uiberacker, W. Jakubetz, in preparation) we will make use of the properties of pulse-train driven mp excitation to demonstrate pulse-train control of resonance leaking [36,40–42] and intruder state population.

Finally we note that while we concentrate on gaussian pulses and sub-pulses considered as "finite" (*i.e.* the fields are cut off when they become negligibly weak in the context of the transitions driven), the results can be carried over to other shapes, such as sine-square- or plateau-pulses.

Acknowledgement

This work was supported by the Austrian Science Fund within the framework of the Special Research Program F016 "ADLIS".

References

[1] N.V. Vitanov, P.L. Knight, Phys. Rev. A 52 (1995) 2245.
[2] R.J. Temkin, J. Opt. Soc. Am. B 10 (1993) 830.
[3] D. Felinto, C.A.C. Bosco, L.H. Acioli, S.S. Vianna, Opt. Commun. 215 (2003) 69.
[4] S. Besnainou, J.-C. Diels, J. Stone, J. Chem. Phys. 81 (1984) 143.
[5] J.-C. Diels, S. Besnaiou, J. Chem. Phys. 85 (1986) 6347.
[6] A.M. Weiner, D.E. Leaird, G.P. Wiederrecht, K.A. Nelson, J. Opt. Soc. Am. B 8 (1991) 1264.
[7] D. Felinto, C.A.C. Bosco, L.H. Acioli, S.S. Vianna, Phys. Rev. A 64 (2001) 063413.
[8] D. Felinto, L.H. Acioli, S.S. Vianna, Phys. Rev. A 70 (2004) 043403.
[9] W. Yang, Sh. Gong, R. Li, Zh. Xu, Phys. Rev. A 74 (2006) 013407.
[10] A. Pe'er, E.A. Shapiro, M.C. Stowe, M. Shapiro, J. Ye, Phys. Rev. Lett. 98 (2007) 113004.
[11] L. Allen, J.H. Eberly, Optical Resonance and Two Level Atoms, Wiley, New York, 1975.
[12] S. Chelkowski, A.D. Bandrauk, P.B. Corkum, Phys. Rev. Lett. 65 (1990) 2355.
[13] M. Holthaus, B. Just, Phys. Rev. A 49 (1994) 1950.
[14] M. Grifoni, P. Hänggi, Phys. Rep. 304 (1998) 229.
[15] S. Guérin, H.R. Jauslin, Eur. Phys. J. D 2 (1998) 99.
[16] S. Guérin, L.P. Yatsenko, H.R. Jauslin, Phys. Rev. A 63 (2001) 031403.
[17] Th. Udem, J. Reichert, R. Holzwarth, T.W. Hänsch, Opt. Lett. 24 (1999) 681.
[18] G.K. Paramonov, V.A. Savva, Chem. Phys. Lett. 107 (1984) 394.
[19] G.K. Paramonov, V.A. Savva, Opt. Commun. 52 (1984) 69.
[20] B.G. Dibble, R.B. Shirts, J. Chem. Phys. 94 (1991) 3451.
[21] G.F. Thomas, Phys. Rev. A 35 (1987) 5060.
[22] G.F. Thomas, Phys. Rev. A 41 (1990) 1645.
[23] J.M. Bowman, B. Gazdy, J.A. Bentley, T.J. Lee, C.E. Dateo, J. Chem. Phys. 99 (1993) 308.
[24] H. Shull, G.G. Hall, Nature 184 (1959) 1559.
[25] W. Jakubetz, B.-L. Lan, Chem. Phys. 217 (1997) 375.
[26] P. Botschwina, M. Horn, M. Matuschewski, E. Schick, P. Sebald, J. Mol. Struct. (THEOCHEM) 400 (1997) 119.
[27] T. van Mourik, G.J. Harris, O.L. Polyansky, J. Tennyson, A.G. Csaszar, P.J. Knowles, J. Chem. Phys. 115 (2001) 3706.
[28] S. Nakai, W.J. Meath, J. Chem. Phys. 96 (1992) 4991.
[29] B.N. Jagatap, W.J. Meath, J. Opt. Soc. Am. B 19 (2002) 2673.
[30] A. Datta, C.A. Marx, C. Uiberacker, W. Jakubetz, Chem. Phys. 338 (2007) 237.
[31] F. Bloch, A. Siegert, Phys. Rev. 57 (1940) 522.
[32] P.K. Aravind, J.O. Hirschfelder, J. Phys. Chem. 88 (1984) 4788.
[33] I.I. Rabi, Phys. Rev. 51 (1937) 652.
[34] K. Drese, M. Holthaus, Eur. Phys. J. D 3 (1998) 73.
[35] N.F. Scherer, R.J. Carlson, A. Matro, M. Du, A.J. Ruggiero, V. Romerorochin, J.A. Cina, G.R. Fleming, S.A. Rice, J. Chem. Phys. 95 (1991) 1487.
[36] W. Jakubetz, B.-L. Lan, J. Chem. Phys. 117 (2002) 7968.
[37] W. Zhu, J. Botina, H. Rabitz, J. Chem. Phys. 108 (1998) 1953.
[38] W. Zhu, H. Rabitz, J. Chem. Phys. 119 (2003) 3619.
[39] G. Gerber, T. Brixner, M. Wollenhaupt, T. Baumert, in: P. Hannaford (Ed.), Femtosecond Laser Spectroscopy, Kluwer, Dordrecht, 2004, p. 229.
[40] T. Uzer, W.H. Miller, Phys. Rep. 199 (1991) 73.
[41] B.-L. Lan, I. Vrábel, W. Jakubetz, J. Chem. Phys. 121 (2004) 10401.
[42] M. Etinski, C. Uiberacker, W. Jakubetz, J. Chem. Phys. 124 (2006) 124110.